

# Giant Magnetic Anisotropy Induced by Ligand $LS$ Coupling in Layered Cr Compounds

Dong-Hwan Kim,<sup>1,2</sup> Kyoo Kim,<sup>2</sup> Kyung-Tae Ko,<sup>1,2</sup> JunHo Seo,<sup>1,3</sup> Jun Sung Kim,<sup>1,3</sup> Tae-Hwan Jang,<sup>2</sup> Younghak Kim,<sup>4</sup> Jae-Young Kim,<sup>3</sup> Sang-Wook Cheong,<sup>5,6</sup> and Jae-Hoon Park<sup>1,2,7,\*</sup>

<sup>1</sup>Department of Physics, POSTECH, Pohang 37673, Korea

<sup>2</sup>MPPHC-CPM, Max Planck POSTECH/Korea Research Initiative, Pohang 37673, Korea

<sup>3</sup>Center for Artificial Low Dimensional Electronic Systems, IBS, Pohang 37673, Korea

<sup>4</sup>Pohang Accelerator Laboratory, POSTECH, Pohang 37673, Korea

<sup>5</sup>Laboratory for Pohang Emergent Materials and Max Planck POSTECH Center for Complex Phase Materials, POSTECH, Pohang 37673, Korea

<sup>6</sup>Rutgers Center for Emergent Materials and Department of Physics and Astronomy, Rutgers University, Piscataway, New Jersey 08854, USA

<sup>7</sup>Division of Advanced Materials Science, POSTECH, Pohang 37673, Korea



(Received 10 August 2018; published 24 May 2019)

We propose a novel origin of magnetic anisotropy to explain the unusual magnetic behaviors of layered ferromagnetic Cr compounds ( $3d^3$ ) wherein the anisotropy field varies from  $\lesssim 0.01$  to  $\sim 3$  T on changing the ligand atom in a common hexagonal structure. The effect of the ligand  $p$  orbital spin-orbit ( $LS$ ) coupling on the magnetic anisotropy is explored by using four-site full multiplet cluster model calculations for energies involving the superexchange interaction at different spin axes. Our calculation shows that the anisotropy energy, which is the energy difference for different spin axes, is strongly affected not only by the  $LS$  coupling strength but also by the degree of  $p$ - $d$  covalency in the layered geometry. This anisotropy energy involving the superexchange appears to dominate the magnetic anisotropy and even explains the giant magnetic anisotropy as large as 3 T observed in  $\text{CrI}_3$ .

DOI: [10.1103/PhysRevLett.122.207201](https://doi.org/10.1103/PhysRevLett.122.207201)

Quantum fluctuation becomes more effective in low-dimensional magnetic systems and often realizes exotic quantum ground states such as the spin-1 Haldane gap state in one dimension (1D) chain systems [1,2] and the spin liquid state with anyonic excitation in 2D layered Kitaev systems [3–5], differently from the ordinary ferromagnetic or antiferromagnetic ordered ground state. The Mermin-Wagner theorem even tells us that no long-range order can persist in the 2D Heisenberg magnetic system due to the strong spin fluctuation [6]. Meanwhile, the magnetically ordered ground state has been observable in several 2D-like layered systems and attributed to an imperfection of the two-dimensionality caused by nonvanishing interlayer coupling in real materials [7–11].

Recently, true 2D ferromagnetism has been realized in single-layer  $\text{CrI}_3$  [12] and also in  $\text{Cr}_2\text{Ge}_2\text{Te}_6$  pristine double layers [13]. Considering the  $\text{Cr}^{3+}$  ( $t_{2g}^3$ ;  $^4A_2$ ) ionic state with minimal orbital angular momentum ( $L \simeq 0$ ), these discoveries are surprising, since the magnetocrystalline anisotropy ( $\xi \mathbf{L} \cdot \mathbf{S}$ ) is sufficiently small for the system to be considered as a near-Heisenberg magnetic system. On the other hand, bulk  $\text{CrI}_3$  has been observed to exhibit giant magnetic anisotropy energy. This strong anisotropy is speculated to suppress the spin fluctuation significantly to realize ferromagnetism even in a true 2D system [12,13]. However, the presence of giant magnetic anisotropy itself

in Cr compounds with  $L \simeq 0$  contradicts current explanations on the magnetic anisotropy, and its origin has been puzzling.

$\text{CrX}_3$  ( $X = \text{Cl}, \text{Br}, \text{and I}$ ) and  $\text{CrYTe}_3$  ( $Y = \text{Ge and Si}$ ) are commonly crystallized in the  $R\bar{3}$  rhombohedral structure [14–19]. Figure 1(a) shows the 2D atomic arrays of

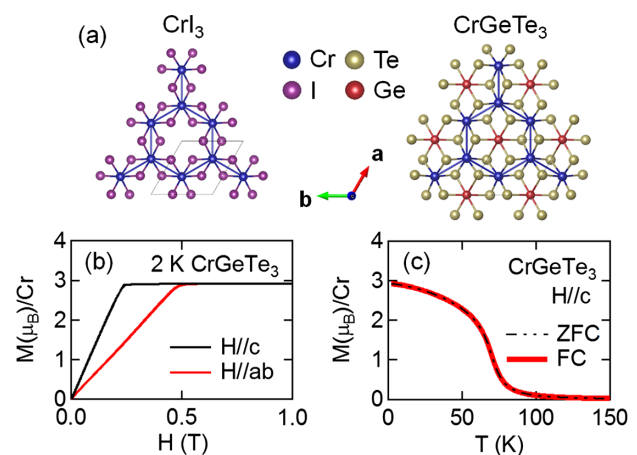


FIG. 1. (a) Top views of  $\text{CrI}_3$  (left) and  $\text{CrGeTe}_3$  (right) layers. Cr, I, Ge, and Te are represented by blue, purple, red, and yellow spheres, respectively. (b)  $M$ - $H$  curves corresponding to  $H\parallel c$  and  $H\parallel ab$  and (c)  $M$ - $T$  curves measured on  $\text{CrGeTe}_3$ . Field cooling (FC) was processed under  $H = 0.5$  T.

CrI<sub>3</sub> and CrGeTe<sub>3</sub> as representatives of both systems. Both structures are the so-called 1T AB<sub>2</sub> layered structure, in which one out of three A sites is empty (CrX<sub>3</sub>) or replaced with a Ge or Si dimer (CrYTe<sub>3</sub>). The trigonal distortion of CrX<sub>6</sub> octahedra is minimal in CrX<sub>3</sub>, while the inserted dimer in CrYTe<sub>3</sub> considerably elongates the CrTe<sub>6</sub> octahedron along the trigonal (hexagonal) *c* axis.

These Cr compounds are all magnetic insulators with a local magnetic moment near  $3\mu_B/\text{Cr}$ , of which the intra-layer interaction is ferromagnetic [14,19–24], as expected in the Goodenough-Kanamori rule for the 90° superexchange hopping path [25–27]. The interlayer coupling is ferromagnetic except in the case of CrCl<sub>3</sub>, in which it is antiferromagnetic but sufficiently weak for the ordering to become ferromagnetic even under a small magnetic field ( $<0.01$  T) [18,22]. Such a minimal interlayer interaction was also reported in inelastic neutron scattering and critical exponent analysis studies on other layered Cr compounds such as CrBr<sub>3</sub> and CrYTe<sub>3</sub> [28–31]. These layered ferromagnets, including CrCl<sub>3</sub>, commonly exhibit a soft magnet behavior of a linear *M-H* curve before saturation with either zero or a minimal ( $<0.01$  T) coercive field [18–22,29,32] and zero deviation in the field cooling in the *M-T* curve, as shown in Figs. 1(b) and 1(c) for CrGeTe<sub>3</sub> as an example, respectively. Similar magnet behaviors were also reported in other quasi-2D ferromagnets such as Fe<sub>3</sub>GeTe<sub>2</sub> and K<sub>2</sub>CuF<sub>4</sub> [33,34].

In addition to the soft magnet behaviors, we can also observe a large difference in the saturation magnetic field for  $H\parallel c$  ( $H_c^S$ ) and  $H\parallel ab$  ( $H_{ab}^S$ ), as shown in Fig. 1(b). Remarkably, the anisotropy field  $\Delta H^S = H_c^S - H_{ab}^S$  varies from  $\lesssim 0.01$  T (CrCl<sub>3</sub>) to  $\sim 3$  T (CrI<sub>3</sub>) on changing only the ligand environment (see Table S1 in Supplemental Material [35]). This large variation contradicts the general explanation with two leading terms of the single-ion (magnetocrystalline) and shape (dipole-dipole) magnetic anisotropies, which are too small to explain the variation. The single-ion anisotropy originates from anisotropy in *L*, mostly quenched in the Cr<sup>3+</sup>  $t_{2g}^3$  ( $4A_2;^4S$ ) compounds, with the energy  $\Delta E_{LS} = -\xi \Delta L S/4$ . The Cr 3*d* *LS* coupling energy  $\xi \mathbf{L} \cdot \mathbf{S}$  partially admixes the  $t_{2g}$  and  $e_g$  orbitals to restore small values of  $L \sim 2\xi/10 \text{ Dq} \simeq 0.06$  for  $\xi(\text{Cr}3d) \simeq 30 \text{ meV}$  and  $10 \text{ Dq} \sim 1 \text{ eV}$ . Indeed, we obtained  $L \sim 0.05$  and one or 2 orders of magnitude smaller  $\Delta L$  values in both the Cr *L*<sub>2,3</sub>-edge x-ray magnetic circular dichroism (XMCD) measurements and the theoretical cluster model calculations [35]. The resulting  $\Delta E_{LS}$  is  $\sim 0.04 \text{ meV}$  ( $\sim 0.2 \text{ T}$ ) for CrGeTe<sub>3</sub> and  $\sim 0.004 \text{ meV}$  ( $\sim 0.02 \text{ T}$ ) for CrI<sub>3</sub>. The shape anisotropy commonly favors the in-plane easy axis in the layered materials. The magnitude is roughly  $\Delta E_{\text{dipole}} \simeq \mu_0 m^2 / 4\pi r^3 \sim 0.02 \text{ meV}$  ( $\sim 0.1 \text{ T}$ ).

Figure 2 displays the magnetic anisotropy energy  $\Delta E_K = 3\mu_B \Delta H^S$  at a low temperature as a function of the ligand *p* spin-orbit coupling strength  $\xi_p$ . Interestingly,  $|\Delta H^S|$  greatly increases with an increase in  $\xi_p$  except

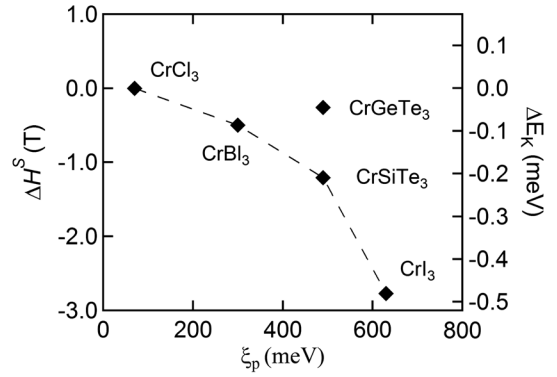


FIG. 2. Anisotropy fields  $\Delta H^S$  and magnetic anisotropy energies  $\Delta E_K$  of various layered Cr compounds, CrCl<sub>3</sub> [18,22], CrBr<sub>3</sub> [21], CrI<sub>3</sub> [19], CrGeTe<sub>3</sub> [29], and CrSiTe<sub>3</sub> [32], as a function of the ligand *p* spin-orbit coupling strength  $\xi_p$ .

for CrGeTe<sub>3</sub>, thus implying that significant magnetic anisotropy is additionally contributed by the ligand *p* electrons. Indeed, a recent first principles band calculation study on CrI<sub>3</sub> suggested the role of I 5*p* spin-orbit coupling to explain the giant magnetic anisotropy [41]. One may suspect a possible contribution of the single-ion anisotropy via the ligand *p* state, which is also spin polarized through hybridization with the Cr 3*d* state. However, the ligand *p* single-ion anisotropy turns out to be negligible in the I *M*<sub>4,5</sub>-edge (I 3*d* → 5*p*) XMCD study on CrI<sub>3</sub> with the largest  $\xi_p$  value of 0.63 eV (see Fig. S3 in Supplemental Material [35]).

Another possibility to consider could be a magnetic anisotropy term contributed by  $\xi_p$  through Cr 3*d*-ligand *p*-Cr 3*d* superexchange hopping in the near 90° bonding angle networks. The large  $\xi_p$  splits the ligand *p* state into the total angular momentum  $j_{3/2}$  and  $j_{1/2}$  states. As an example, let us consider the Cr  $d_{yz}$ -ligand  $p_{j_{1/2}}$ -Cr  $d_{3x^2-r^2}$  superexchange electron hopping channel for two different spin axes,  $\mathbf{M}\parallel\hat{y}$  and  $\mathbf{M}\parallel\hat{z}$ , as depicted in Figs. 3(a) and 3(b), respectively. Here,  $|j = 1/2, m_j = -1/2\rangle$  was chosen for the ligand  $p_{j_{1/2}}$  on purpose (the hopping actually vanishes for  $|1/2, +1/2\rangle$ ). This  $j_{1/2}$  state is an admixed state in both spin and orbital states and is represented as  $(p_{x,+\sigma_z} - ip_{y,+\sigma_z} - p_{z,-\sigma_z})/\sqrt{3}$  in the conventional  $\hat{z}$ -spin axis, i.e.,  $\mathbf{M}\parallel\hat{z}$ . However, when the spin axis changes to the  $\hat{y}$  axis, the  $j_{1/2}$  state becomes  $(p_{z,+\sigma_y} - ip_{x,+\sigma_y} - p_{y,-\sigma_y})/\sqrt{3}$ . Here,  $\pm\sigma_y$  and  $\pm\sigma_z$  denote the up and down spin along the  $\hat{y}$ - and  $\hat{z}$ -spin axes, respectively.

The hopping channel is represented by consecutive electron hoppings of the ligand *p* to 3*d* in one Cr site through ligand  $p(j_{1/2})$ -Cr  $e_g$  ( $d_{3x^2-r^2}$ ) hybridization and  $t_{2g}$  in the other Cr site to ligand *p* ( $j_{1/2}$ ) through  $d_{yz}$ - $j_{1/2}$  hybridization. We note that the orbital-geometry symmetry allows only the  $p_x$ - $d_{3x^2-r^2}$  ( $pd\sigma$ ) and  $d_{yz}$ - $p_z$  ( $pd\pi$ ) hybridizations. Considering that the hybridization is spin independent,  $d_{yz}$ - $p_z$  hybridization vanishes for  $\mathbf{M}\parallel\hat{z}$  due to their different spin states,  $+\sigma_z$  and  $-\sigma_z$ , respectively. As a result,

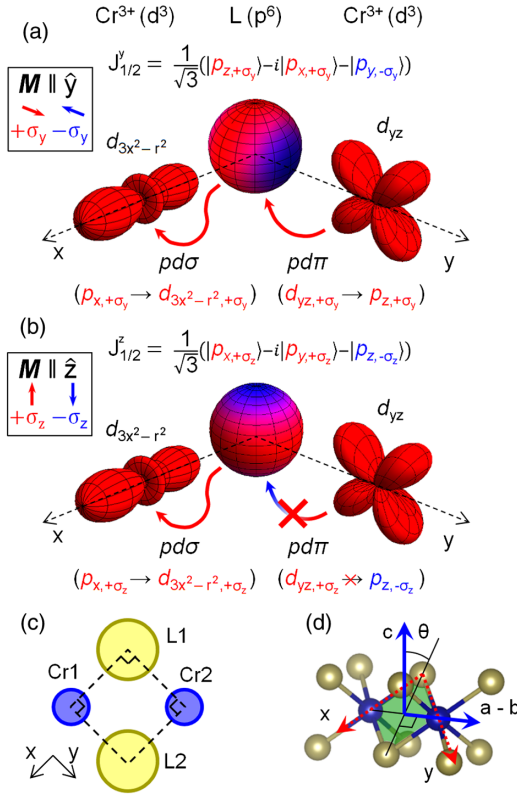


FIG. 3. Cr  $d_{yz}$ -L  $p_{j1/2}$ -Cr  $d_{3x^2-r^2}$  superexchange for (a)  $\mathbf{M} \parallel \hat{y}$  and (b)  $\mathbf{M} \parallel \hat{z}$ . The spin states are indicated by red ( $+\sigma_{y,z}$ ) and blue ( $-\sigma_{y,z}$ ) colors. (c) Two equivalent  $90^\circ$  superexchange paths through ligands (L1 and L2) between two adjacent Cr atoms. (d) Cr-L-Cr local network (red dashed line) in the crystal coordinates (a and c).

superexchange hopping is allowed only for the spin axis  $\mathbf{M} \parallel \hat{y}$  though nonvanishing  $p_{x+\sigma_y}$ - $d_{3x^2-r^2,+\sigma_y}$  and  $d_{yz,+\sigma_y}$ - $p_{z,+\sigma_y}$  hybridizations. Therefore, this superexchange hopping path contributes a magnetic anisotropy term favoring  $\mathbf{M} \parallel \hat{y}$  (in plane). The magnetic anisotropy contribution varies with the hopping channel, and the net magnetic anisotropy, the so-called magnetic exchange anisotropy, can be determined by summing the contributions for all possible Cr  $t_{2g}$ , ligand  $p$ , Cr  $e_g$  orbital combination channels of the superexchange hopping.

In layered Cr compounds, two equivalent ligands exist between two neighboring Cr sites with a near  $90^\circ$  bonding angle. Thus, we performed full multiplet cluster calculations for a four-site ansatz in the edge-shared plane consisting of two Cr and two ligand sites [Fig. 3(c)] to quantify the magnetic exchange anisotropy. In the calculation, we took into account the full atomic multiplets as well as all configurations up to charge transferred three-hole states at the ligand sites (see Supplemental Material, Sec. III [35], for details). In the layered Cr compounds, the edge-shared (xy) plane has an off-angle  $\theta$  from the crystal c axis as shown in Fig. 3(d). Angle  $\theta$  in the crystal structure, which slightly deviates from  $\theta_{Oh} \simeq 35.3^\circ$  by the degree of

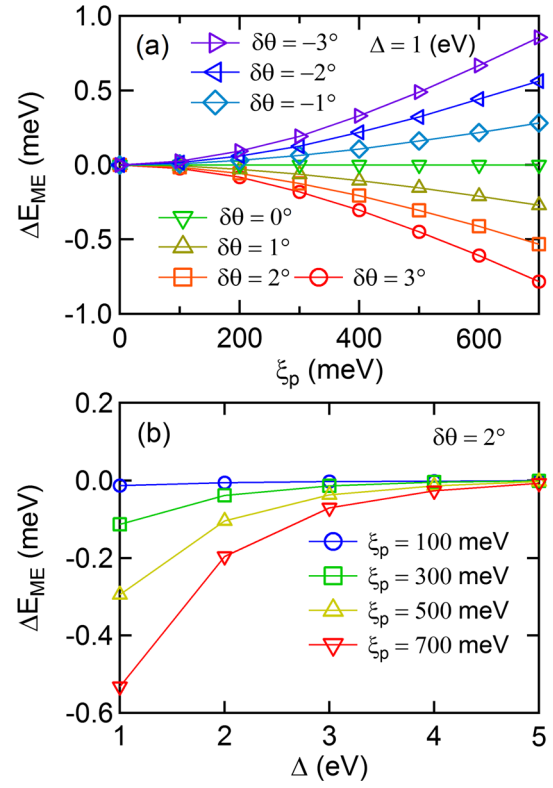


FIG. 4. Four-site full multiplet cluster model calculation results for  $\Delta E_{ME}$  as functions of (a)  $\xi_p$  for various  $\delta\theta$  values at  $\Delta = 1$  eV and of (b)  $\Delta$  for various  $\xi_p$  values at  $\delta\theta = 2^\circ$ .

trigonal distortion, is utilized for the determination of the net magnetic exchange anisotropy  $\Delta E_{ME} = E_{ME}^c - E_{ME}^{ab}$ , which vanishes at the deviation angle  $\delta\theta = \theta_{Oh} - \theta = 0$ .

Figure 4 displays the calculated  $\Delta E_{ME}$  as a function of (a)  $\xi_p$  for different  $\delta\theta$  values and of (b) ligand  $p$  to Cr 3d charge transfer energy  $\Delta$  for different  $\xi_p$  values. Here, the number ( $z = 3$ ) of equivalent neighboring Cr sites is taken into account. Parameter values such as the 3d on-site Coulomb energy  $U_{dd}$  and the hybridization strengths  $p_{d\sigma}/p_{d\pi}$  are taken from the cluster model analyses of the Cr  $L_{2,3}$ -edge XAS/XMCD results of  $\text{CrI}_3$  (see Table S2 in Supplemental Material [35]). Since  $\Delta E_{ME}$  basically originates from the spin-axis-dependent superexchange hopping in the hexagonal structure, its magnitude is mainly determined by three factors: the degree of spin state mixing involving  $\xi_p$ , the superexchange energy scale varying with  $\Delta$ , and the geometry factor in the exchange anisotropy in the hexagonal structure [see Fig. 3(d)] represented with  $\delta\theta$  driven by the trigonal distortion, resulting in a power law form of  $\Delta E_{ME} \propto (\xi_p)^\alpha (\delta\theta)^\beta / (\Delta)^\gamma$ . Indeed, the full calculation results turn out to be suitably represented by this form with  $\alpha \simeq 1.7$ ,  $\beta \simeq 1$ , and  $\gamma = 1.5-1.9$  (see Supplemental Material, Sec. IV [35]). For a given  $\Delta$  value,  $\Delta E_{ME}$  increases with  $\xi_p$  and reaches up to 0.9 meV for  $\xi_p = 700$  meV and  $\delta\theta = 3^\circ$ . This means that  $\Delta E_{ME}$  is sufficiently large to explain the largest anisotropy energy



TABLE I. Parameters used in model calculations and magnetic anisotropy energies obtained from calculations as described in the text. Here,  $\delta E_K = \Delta E_{LS} + \Delta E_{\text{dipole}}$ .

	CrCl <sub>3</sub>	CrBr <sub>3</sub>	CrI <sub>3</sub>	CrGeTe <sub>3</sub>	CrSiTe <sub>3</sub>
$\xi_p$ (meV)	70	300	630	490	490
$\delta\theta$ (°)	2	2	2	7	7
$\Delta$ (eV)	3.5	1.5	1.2	2.2	2.2
$\Delta E_{\text{ME}}$ (meV)	$\lesssim 0.001$	-0.084	-0.47	-0.27	-0.27
$\Delta'$ (eV)	None	None	None	1.3	2.0
$\Delta E'_{\text{ME}}$ (meV)	None	None	None	0.17	0.01
$\delta E_K$ (meV)	0.01	0.01	0.01	0.06	0.06
$\Delta E_K^{\text{th}}$ (meV)	0.01	-0.074	-0.46	-0.040	-0.21
$\Delta E_K^{\text{exp}}$ (meV)	$\lesssim 0.001$	-0.086	-0.48	-0.045	-0.21

$\Delta E_K \sim 0.5$  meV required for CrI<sub>3</sub> (see Fig. 2), which has  $\xi_p = 630$  meV and  $\delta\theta \simeq 2^\circ$ . Indeed, the observed magnetic anisotropy  $\Delta E_K^{\text{exp}}$  agrees closely with the estimated  $\Delta E_{\text{ME}}$  with reasonable  $\Delta$  for CrX<sub>3</sub> and CrSiTe<sub>3</sub> with different ligands after correction  $\delta E_K = \Delta E_{LS} + \Delta E_{\text{dipole}}$  of the single-ion and shape anisotropy contributions estimated from the XMCD and numerical magnetic dipole energy analyses, as summarized in Table I. The correction is somewhat large in CrYTe<sub>3</sub> by its sizable  $\Delta E_{LS}$  ( $\sim 0.04$  meV) resulting from the greatly elongated CrTe<sub>6</sub> octahedron due to the inserted A-site dimer.

Despite the fact that CrGeTe<sub>3</sub> has the same Te ligands as CrSiTe<sub>3</sub>, its  $\Delta E_K$  is reduced significantly from that of CrSiTe<sub>3</sub>, thus indicating that the A-site dimer considerably affects the electronic structure of the Te 5p states. In fact, the Ge or Si dimer forms a strong covalent bond with Te to split the Te 5p band into the bonding (occupied) and antibonding (unoccupied) states. As a result, the ordinary Te 5p to Cr 3d charge transfer energy  $\Delta$  effectively increases, and a new charge transfer from Cr 3d to the unoccupied Te 5p is introduced. Figure 5 presents the

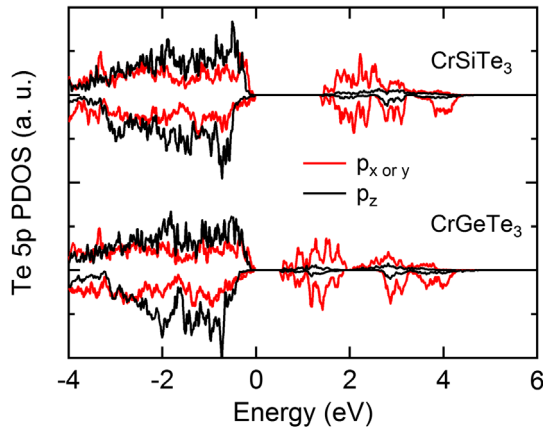


FIG. 5. Partial density of state of Te 5p orbitals determined from wannierization on CrGeTe<sub>3</sub> and CrSiTe<sub>3</sub>. Strong Si(Ge)-Te covalent bonding effectively pushes down the occupied bonding states by about 1.5 eV (weighted average) and transfers about 30% Te 5p weight to the unoccupied antibonding states.

density of states (DOS) of the Te 5p orbital states for CrGeTe<sub>3</sub> and CrSiTe<sub>3</sub> obtained from the wannierized band structure calculations in the absence of Cr 3d-Te 5p hybridization [35], which is explicitly taken into account in the cluster model calculations. As can be seen in the figure, the occupied Te 5p states are nearly the same in energy for these compounds, while a significant energy difference appears for the unoccupied states. The Cr 3d to the unoccupied Te 5p charge transfer energy  $\Delta'$  of CrGeTe<sub>3</sub> is estimated to be smaller by 0.7 eV than that of CrSiTe<sub>3</sub> through weighted averaging. This new charge transfer opens additional Cr 3d-unoccupied Te 5p-Cr 3d superexchange channels and contributes an additional magnetic exchange anisotropy, which significantly reduces the magnetic anisotropy  $\Delta E_K$  in CrGeTe<sub>3</sub> as can be inferred from Table I.

We have thus far demonstrated that the additional magnetic exchange anisotropy, induced by the ligand p spin-orbit coupling through the superexchange mechanism, suitably explains the large variation in the magnetic anisotropy energy of layered Cr compounds and is also responsible for the giant magnetic anisotropy observed in CrI<sub>3</sub> and CrSiTe<sub>3</sub>. The magnetic exchange anisotropy introduces anisotropy in the spin-spin exchange interaction, thus resulting in an anisotropic Heisenberg spin Hamiltonian of the form

$$H = J_{xx}(S_x^1 S_x^2 + S_y^1 S_y^2) + J_{zz} S_z^1 S_z^2, \quad (1)$$

which leads to the predicted realization of the ferromagnetic ground state in the 2D spin system [42], as observed in these compounds with  $L \simeq 0$ . Our results indicate that the magnetic exchange anisotropy can significantly contribute to the magnetic anisotropy for magnetic systems with large ligand spin-orbit coupling to realize true 2D ferromagnetism, and they also suggest a new approach to search giant magnetic anisotropy materials for potential applications to spintronic devices.

This work was supported by the Max Planck POSTECH/Korea Research Initiative, Study for Nano Scale Optomaterials and Complex Phase Materials (2016K1A4A4A01922028), through the National Research Foundation (NRF) funded by MSIP of Korea. K. K. (NRF-2016R1D1A1B02008461) and K.-T. K. (NRF-2017M2A2A6A01071297) were also supported by NRF, and S.-W. C. was supported by the National Science Foundation (DMR-1629059) of the United States. J. S. K. was supported by the Institute for Basic Science (IBS-R014-D1), POSCO through the Green Science program, and NRF through the SRC program (2011-0030785).

\*Corresponding author.  
jhp@postech.ac.kr

[1] F. D. M. Haldane, *Phys. Rev. Lett.* **50**, 1153 (1983).

- [2] M. Kenzelmann, R. A. Cowley, W. J. L. Buyers, Z. Tun, R. Coldea, and M. Enderle, *Phys. Rev. B* **66**, 024407 (2002).
- [3] A. Kitaev, *Ann. Phys. (Amsterdam)* **321**, 2 (2006).
- [4] A. Banerjee, J. Yan, J. Knolle, C. A. Bridges, M. B. Stone, M. D. Lumsden, D. G. Mandrus, D. A. Tennant, R. Moessner, and S. E. Nagler, *Science* **356**, 1055 (2017).
- [5] S.-H. Do, S.-Y. Park, J. Yoshitake, J. Nasu, Y. Motome, Y. Kwon, D. T. Adroja, D. J. Voneshen, K. Kim, T.-H. Jang, J.-H. Park, K.-Y. Choi, and S. Ji, *Nat. Phys.* **13**, 1079 (2017).
- [6] N. D. Mermin and H. Wagner, *Phys. Rev. Lett.* **17**, 1133 (1966).
- [7] X. Liu, T. Berlijn, W.-G. Yin, W. Ku, A. Tsvelik, Y.-J. Kim, H. Gretarsson, Y. Singh, P. Gegenwart, and J. P. Hill, *Phys. Rev. B* **83**, 220403(R) (2011).
- [8] R. D. Johnson, S. C. Williams, A. A. Haghighirad, J. Singleton, V. Zapf, P. Manuel, I. I. Mazin, Y. Li, H. O. Jeschke, R. Valentí, and R. Coldea, *Phys. Rev. B* **92**, 235119 (2015).
- [9] H. Ikeda and K. Hirakawa, *J. Phys. Soc. Jpn.* **35**, 722 (1973).
- [10] K. M. Kojima, Y. Fudamoto, M. Larkin, G. M. Luke, J. Merrin, B. Nachumi, Y. J. Uemura, N. Motoyama, H. Eisaki, S. Uchida, K. Yamada, Y. Endoh, S. Hosoya, B. J. Sternlieb, and G. Shirane, *Phys. Rev. Lett.* **78**, 1787 (1997).
- [11] H. Kadowaki, K. Ubukoshi, and K. Hirakawa, *J. Phys. Soc. Jpn.* **56**, 751 (1987).
- [12] B. Huang, G. Clark, E. Navarro-Moratalla, D. R. Klein, R. Cheng, K. L. Seyler, D. Zhong, E. Schmidgall, M. A. McGuire, D. H. Cobden, W. Yao, D. Xiao, P. Jarillo-Herrero, and X. Xu, *Nature (London)* **546**, 270 (2017).
- [13] C. Gong, L. Li, Z. Li, H. Ji, A. Stern, Y. Xia, T. Cao, W. Bao, C. Wang, Y. Wang, Z. Q. Qiu, R. J. Cava, S. G. Louie, J. Xia, and X. Zhang, *Nature (London)* **546**, 265 (2017).
- [14] V. Carteaux, D. Brunet, G. Ouvrard, and G. Andre, *J. Phys. Condens. Matter* **7**, 69 (1995).
- [15] R. E. Marsh, *J. Solid State Chem.* **77**, 190 (1988).
- [16] L. L. Handy and N. W. Gregory, *J. Am. Chem. Soc.* **74**, 891 (1952).
- [17] B. Morosin and A. Narath, *J. Chem. Phys.* **40**, 1958 (1964).
- [18] A. A. McGuire, G. Clark, K. C. Santosh, W. M. Chance, G. E. Jellison, V. R. Cooper, X. Xu, and B. C. Sales, *Phys. Rev. Mater.* **1**, 014001 (2017).
- [19] M. A. McGuire, H. Dixit, V. R. Cooper, and B. C. Sales, *Chem. Mater.* **27**, 612 (2015).
- [20] H. Ji, R. A. Stokes, L. D. Alegria, E. C. Blomberg, M. A. Tanatar, A. Reijnders, L. M. Schoop, T. Liang, R. Prozorov, K. S. Burch, N. P. Ong, J. R. Petta, and R. J. Cava, *J. Appl. Phys.* **114**, 114907 (2013).
- [21] J. J. F. Dillon, *J. Phys. Soc. Jpn.* **19**, 1662 (1964).
- [22] A. Narath and H. L. Davis, *Phys. Rev.* **137**, A163 (1965).
- [23] V. Carteaux, G. Ouvrard, J. Grenier, and Y. Laligant, *J. Magn. Magn. Mater.* **94**, 127 (1991).
- [24] I. Tsubokawa, *J. Phys. Soc. Jpn.* **15**, 1664 (1960).
- [25] J. B. Goodenough, *Phys. Rev.* **100**, 564 (1955).
- [26] J. B. Goodenough, *J. Phys. Chem. Solids* **6**, 287 (1958).
- [27] J. Kanamori, *J. Phys. Chem. Solids* **10**, 87 (1959).
- [28] E. J. Samuels, R. Silbergliitt, G. Shirane, and J. P. Remeika, *Phys. Rev. B* **3**, 157 (1971).
- [29] G. T. Lin, H. L. Zhuang, X. Luo, B. J. Liu, F. C. Chen, J. Yan, Y. Sun, J. Zhou, W. J. Lu, P. Tong, Z. G. Sheng, Z. Qu, W. H. Song, X. B. Zhu, and Y. P. Sun, *Phys. Rev. B* **95**, 245212 (2017).
- [30] T. J. Williams, A. A. Aczel, M. D. Lumsden, S. E. Nagler, M. B. Stone, J.-Q. Yan, and D. Mandrus, *Phys. Rev. B* **92**, 144404 (2015).
- [31] B. Liu, Y. Zou, L. Zhang, S. Zhou, Z. Wang, W. Wang, Z. Qu, and Y. Zhang, *Sci. Rep.* **6**, 33873 (2016).
- [32] L. D. Casto, A. J. Clune, M. O. Yokosuk, J. L. Musfeldt, T. J. Williams, H. L. Zhuang, M.-W. Lin, K. Xiao, R. G. Hennig, B. C. Sales, J.-Q. Yan, and D. Mandrus, *APL Mater.* **3**, 041515 (2015).
- [33] K. Kim, J. Seo, E. Lee, K.-T. Ko, B. S. Kim, B. G. Jang, J. M. Ok, J. Lee, Y. J. Jo, W. Kang, J. H. Shim, C. Kim, H. W. Yeom, B. Il Min, B.-J. Yang, and J. S. Kim, *Nat. Mater.* **17**, 794 (2018).
- [34] S. Hirata, N. Kurita, M. Yamada, and H. Tanaka, *Phys. Rev. B* **95**, 174406 (2017).
- [35] See Supplemental Material at <http://link.aps.org/supplemental/10.1103/PhysRevLett.122.207201> for the details about the estimation of magnetic anisotropy energies, which includes Refs. [36,37], and the technical details about the wannierized band structure calculations, which includes Refs. [38–40].
- [36] A. Tanaka and T. Jo, *J. Phys. Soc. Jpn.* **63**, 2788 (1994).
- [37] C. T. Chen, Y. U. Idzerda, H.-J. Lin, N. V. Smith, G. Meigs, E. Chaban, G. H. Ho, E. Pellegrin, and F. Sette, *Phys. Rev. Lett.* **75**, 152 (1995).
- [38] I. Souza, N. Marzari, and D. Vanderbilt, *Phys. Rev. B* **65**, 035109 (2001).
- [39] P. Giannozzi *et al.*, *J. Phys. Condens. Matter* **21**, 395502 (2009).
- [40] R. Sakuma, *Phys. Rev. B* **87**, 235109 (2013).
- [41] J. L. Lado and J. Fernández-Rossier, *2D Mater.* **4**, 035002 (2017).
- [42] E. E. Reinehr and W. Figueiredo, *Phys. Rev. B* **52**, 310 (1995).